Achour, Lazhar; Bouharkat, Malek; Behar, Omar

Article

Performance assessment of an integrated solar combined cycle in the southern of Algeria

Energy Reports

Provided in Cooperation with:
Elsevier

Suggested Citation: Achour, Lazhar; Bouharkat, Malek; Behar, Omar (2018) : Performance assessment of an integrated solar combined cycle in the southern of Algeria, Energy Reports, ISSN 2352-4847, Elsevier, Amsterdam, Vol. 4, pp. 207-217, https://doi.org/10.1016/j.egyr.2017.09.003

This Version is available at:
https://hdl.handle.net/10419/187870

Energy Reports 4 (2018) 207–217

Contents lists available at ScienceDirect

Energy Reports

journal homepage: www.elsevier.com/locate/egyr

Performance assessment of an integrated solar combined cycle in the southern of Algeria

Lazhar Achour [a,*], Malek Bouharkat [a], Omar Behar [b]

[a] Electrical Engineering Department, University of Batna, Batna, Algeria
[b] University of M'Hammed Bougara, UMBB, Boumerdes, Algeria

HIGHLIGHTS

- It is to assess the performance on an ISCC.
- A simple model to estimate the DNI is suggested.
- A thermodynamic model is then highlighted.
- Solar to electricity efficiency has been discussed.

ARTICLE INFO

Article history:
Received 12 October 2016
Received in revised form 5 September 2017
Accepted 20 September 2017

Keywords:
ISCC
CSP
Solar thermal power plant
Hybrid solar thermal power plant
Solar radiation

ABSTRACT

Among all the hybrid solar thermal technologies available up to now, the Integrated Solar Combined Cycle (ISCC) is nowadays the most efficient system for converting solar energy into electricity. This power plant is a combination of a parabolic trough solar field with a conventional combined cycle. In the present article, the performance of an ISCC plant under southern Algerian climate has been investigated. To do so, a thermodynamic model has been developed to evaluate solar radiation intensity as well as the overall performance of the hybrid solar power plant.

The analysis has shown that solar to electricity efficiency could reach up to 14.4% during sunny periods. Furthermore, an overall thermal efficiency of about 60% is feasible. It has also been found that the amount of electricity produced increases with several operation parameters such as the time of the day, the mass flow rate of the heat transfer fluid and the angle of incidence on the collector surface.

1. Introduction

The use of parabolic trough technology for power generation and mechanical drive applications is dated as far back as 1913. At this year, the first solar power plant has been built in Al Maadi, Egypt for pumping water irrigation (Duffie and Beckman, 1991; Raafat, 1994). More than one century later (during the 1980s), nine Solar Electric Generating Systems (SEGSs) have been installed in California desert. Then years after, the integration of parabolic trough technology into the fossil fuel combined cycle has been introduced to improve solar energy conversion. The combination of solar field with a combined cycle results in the so called Integrated Solar Combined Cycle (ISCC). This concept has attracted much more interest during the last decade. Typical ISCC is illustrated in Fig. 1. It mainly consists of two gas turbines, an oversized steam turbine and a large parabolic trough solar field.

The first analysis of the ISCC in Tunisia has been carried out by Allani et al. (1997). The authors have obtained that the ISCC is more profitable than SEGS. Dersch et al. (2004) have used GateCycle and IPSEpro in order to compare the performance of the ISCC to SEGS and Combined Cycle (CC) power plants. They have concluded that the ISCC is the most efficient. Kane and Favrat (1999) have focused on the heat exchangers of the ISCC. They have proved that the ISCC with double pressure-reheat and smaller solar field provides better performance.

Bakos and Parsa (2013) have used TRNSYS-STEC software for the economic assessment of the ISCC in Southern Greece. It has been found that the ISCCS more cost-effective. Cau et al. (2012) have also used the GateCycle to analysis the performance of the proposed innovative concept of the ISCC with CO2 as a HTF. The results have shown that the solar energy conversion efficiency is around 25%. Li and Yang (2014) have compared an (ISCC) of two-stage solar input with one-stage. Where the proposed configuration of (ISCC) with two-stage solar input improves the solar-to-electricity efficiency by 1.2%. And later, Li and Yang (2015)

* Corresponding author.
E-mail address: achour_lazhar@yahoo.fr (L. Achour).

https://doi.org/10.1016/j.egyr.2017.09.003

Nomenclature

A	Area, (m^2)
N_c	Number of collectors
H_h	Monthly mean daily global solar irradiation on a horizontal surface (kWh/m^2·day)
$H_{d,h}$	Monthly mean daily diffuse solar irradiation on a horizontal surface (kWh/m^2·day)
H_i	Monthly average daily direct irradiation on a horizontal surface (kWh/ m^2·day)
I_h	Monthly mean hourly global solar irradiation on a horizontal surface (kWh/m^2)
$I_{b,h}$	Monthly mean hourly direct solar irradiation on a horizontal surface (kWh/m^2)
$I_{d,h}$	Monthly mean hourly diffuse solar irradiation on a horizontal surface (kWh/m^2)
I_i	Direct solar irradiation on a tilted surface (W/m^2)
r_t	Daily ratio for global radiation
r_d	Daily ratio for diffuse radiation
LHV	Lower Heating Value, (J/kg)
nj	Number of day of year
n_o	Real day of the year
$\dot{Q}$	Useful energy, (MWth)
W_C W_G and W_{ST}	Compressor, gas and steam turbine works (J/kg)
h_1 h_2 h_3 and h_4	Enthalpy of the steam at the turbine inlet and outlet, enthalpy at the condenser and the pump exit (kJ/kg)
C_{pg}	Specific heat of flue gas (kJ/kg·K)
C_{pa}	Specific heat of air (kJ/kg·K)
$T_{2'}$, $T_{3'}$	Temperature entering and leaving of chamber combustion (K)
$\dot{Q}_{HL,rec}$	Heat loss from the receiver in the solar field (W/m^2)
$\dot{Q}_{HL,pip}$	Heat loss from the pipes in the solar field (W/m^2)
$\dot{Q}_{sol,field}$	Thermal power from the solar field, (MWth)
Q_{fuel}	Fuel energy input (MWth)
Q_{add}	Heat supplied in the combustion (MWth)
Q_{ex}	Heat of exhaust gases in HRSG (MWth)
Q_{SG}	Heat of steam generation (MWth)
N	Power production (MWe)
N_{AUX}	Auxiliary power consumption (MWe)
T	Temperature, (K)
U_0, U_1	Constant determined from empirical test, (W/m^2 °C)
U_L	Heat transfer loss coefficient, (W/m^2·K)
E_{Loss}	Performance factor that accounts for losses from ends of heat collector element
R_{shad}	Performance factor that accounts for mutual shading of parallel collector rows during early morning and late evening
f_{clean}	Cleanliness factor

Greek symbols

$K(i)$	Angle of incidence modifier (°)
i	Angle of incidence (°)
φ	Latitude (°)
δ_s	Declination solar (°)
ω_s	Sunrise hour angle (°)
i_z	Solar zenith angle (°)
$\dot{m}_a$	Air mass flow rate, (kg/s)
$\dot{m}_f$	Fuel mass flow rate, (kg/s)
$\dot{m}_s$	Steam flow rate at the operational condition, (kg/s)
$\dot{m}_g$	Mass flow rate of the exhaust gases, (kg/s)
η_m	Isentropic efficiency of the steam turbine (%)
η_p	Isentropic efficiency of the pump (%)
η_o	Optical efficiency

Subscripts

a	air
amb	ambient
abs	absorber
ap	aperture
c	collector
o	optical
sol	solar
h	hour
min	minute
s	second
f	fluid
in	inlet
out	outlet

Abbreviations

ISCC	Integrated Solar Combined Cycle
IGCC	Integrated Gasification Combined Cycle
CSP	Concentrated Solar Power
CC	Combined Cycle
DNI	Direct Normal Irradiation
GSR	Global Solar Radiation on a horizontal surface data
DSR	Diffuse Solar Radiation on a horizontal surface data
HRSG	Heat Recovery Steam Generator
HSSG	Heat Solar Steam Generator
GT	Gas Turbine
ST	Steam Turbine
FP	Feed water Pump
PTC	Parabolic Trough Collector
HTF	Heat Transfer Fluid
SEGS	Solar electric generating system

proposed a two novel (ISCC), where studied the impacts of solar multiples on system performance with two pressure level DSG solar fields (ISCC-2DSG), with and without of thermal storage. Popov (2014) has been used Thermoflex together with SAM for comparing the two proposed concepts for the ISCC. Where the first one, photovoltaic panels is used to power the inlet cooling system of the gas turbine and is the second one, the inlet cooling system is accomplished with an absorption chiller supplied with DSG Linear Fresnel field. The results showed that the novel configurations provide better thermal efficiency than traditional concept. Baghernejad and Yaghoubi (2011) have suggested a model in MATLAB for the energy and exergy analysis of the ISCC of Yazd, Iran. The simulations have shown that the exergy efficiency of the ISCC can reach 46.8%, while the exergy destruction cost reduced by 14.82%. Khaldi (2012) has proposed a program in Cycle-Tempo for the energy and exergy analysis of the ISCC that have been built in Algeria. The author has found that the energy and the exergy efficiencies of the power plant can achieve 56% and 53% respectively. Derbal-Mokrane et al. (2012) and Behar et al. (2011) have interested on the performance analysis of the ISCC of Hassi R'mel, Algeria. The first authors have used TRNSYS for the simulation, while the second authors have developed a mathematical program using visual FORTRAN. Zhu et al. (2015) developed a model of a three pressure level NGCC with solar integration using the software IPSEpro. They calculated solar thermal-to-electrical efficiencies in

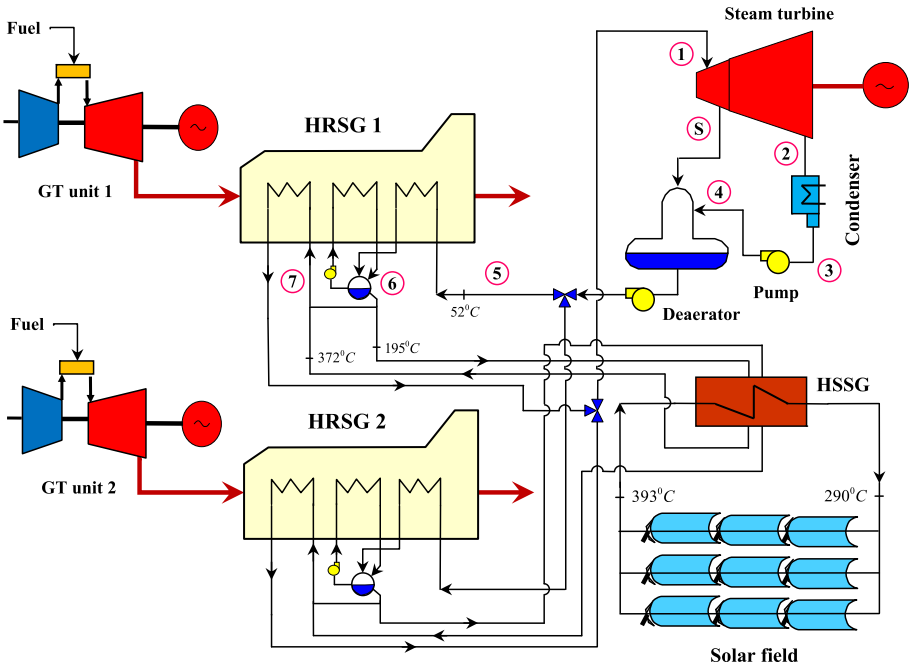

Fig. 1. Typical Integrated Solar Combined Cycle power plant.

the range between 40% and 45% which are significantly higher than the steam cycle efficiency. The overall power boost from solar reached 83MWe which corresponds to a solar share of about 17%.

In a recent study, Manente (2016) has proposed a new concept of ISCC side by side off-design model of a 390 MWe. The author has used Thermoflex software to form the basis of an accurate model. Rovira et al. (2016) used two solar concentration technologies: parabolic trough collectors (PTC) and linear Fresnel reflectors (LFR) to compares the annual performance and economic feasibility of Integrated Solar Combined Cycles (ISCC). The authors have found that the use of Fresnel technology in ISCC is one of the most promising economic results considered both optimistic and conservative scenarios.

Indeed, many researchers have been interested in the investigation of the ISCC performance in Algeria. These authors have selected Hassi R'mel location in the analysis. However, the ambitious renewable energy program of Algeria has expected dozen ISCC's that will be systematically implanted until 2030. Beside Hassi R'mel, many locations in Algerian are considered to hold solar thermal power plants in near future. The present study provides a detailed thermal performance analysis of an ISCC under tropical climate at Tamanrasset (Southern Algeria). An accurate model of seven different modes of tracking has been developed to predict the direct solar irradiance intensity. Then a thermodynamic model is developed including solar field modeling, gas turbine thermodynamic analysis, heat exchanger heat transfer performance and steam turbine modeling.

2. Modeling of solar radiation

As it is highlighted in the renewable energy program that is announced in 2011, Algeria is aimed to develop solar energy to produce about 37% of domestic electricity from both photovoltaics and Concentrating Solar Power (CSP). This is due to the huge potential of solar energy and the longer sunshine duration as it is illustrated in Fig. 2. Therefore the accurate prediction of solar radiation intensity and knowledge of the available solar resource in the country is an important issue for the design of solar energy conversion system. Where solar radiation data are rarely available, it is necessary to develop models to estimate the intensity of solar radiation based on the available climate data. Through previous research, many researchers have been shown that the direct solar radiation is the only used for the nature of the parabolic trough collector.

Table 1
General informations of study area.

Country		Algeria
Station		Tamanrasset
Climate and climatic zone		hot, desert (IV, 5)
Latitude (N)		22°47′N (22.78°)
Longitude (E)		5°31′E (5.517°)
Elevation (m)		1377
WMO Index		606,800
Temperature	T_{min} (°C)	12.9
	T_{max} (°C)	30.0
	Ave (°C)	22.9

In the present study, a simple model has been suggested to estimate the direct component of solar irradiation under Algerian climate. This model is based on the total hourly, daily and monthly direct radiation incident on seven different oriented solar concentrators were calculated, using only the recorded data of monthly mean daily global and diffuse horizontal solar irradiance for Tamanrasset city in Algeria. Algerian National Office of Meteorology (NOM) data of GSR and DSR (kWh/m^2·day) that have been recorded at Tamanrasset location is used in the present study. The geographical and climatic characteristics of the selected location are reported in Table 1.

The seven different tracking systems are shown in below.

C1: A fixed surface south facing (Besarati et al., 2013),

C2: A surface rotated about a horizontal north–south axis (Goswami et al., 2000),

C3: A surface rotated about a horizontal east–west axis (Goswami et al., 2000),

C4: A surface oriented at an angle γ with the south, with a tilt angle of 45° (El Mghouchi et al., 2014)),

C5: A surface tilted at the latitude angle with East–West tracking (Besarati et al., 2013),

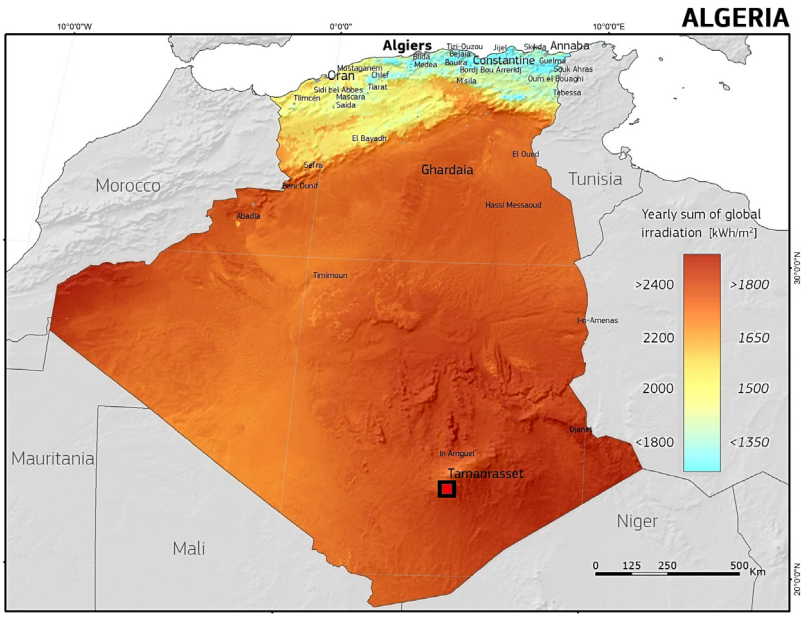

Fig. 2. Solar energy potential in Algeria.

C6: A surface tilted at the latitude angle with azimuth tracking (Goswami et al., 2000),

C7: A surface oriented with azimuth/elevation tracking axis (Goswami et al., 2000),

In the present work, to estimate the direct normal solar radiation and to compare the different models of tracking, we take the data of monthly mean GSR and DSR (kWh/m^2·day) of clear sky radiation from Algerian National Office of Meteorology (NOM). The declination angle δ_s, the monthly mean hourly direct solar irradiation intercepted by the concentrator aperture, were calculated from the standard following relations:

2.1. The day of the year

The day of the year *nj* is calculated taking into account the hour of the day; it can be calculated by the formula:

$$nj = n_0 + \frac{1}{24} \cdot (h + \min 60 + \frac{s}{3600}). \quad (1)$$

This formula gives time in seconds.

2.2. Declination and sunrise hour angles

The declination (δ_s) and the sunrise hour angles (ω_s) are defined by the following equations (Duffie and Beckman, 1991):

$$\delta_s = 23.45^\circ \sin(\frac{360(284 + nj)}{365}) \quad (2)$$

$$\omega_s = arcos(-\tan\varphi \cdot \tan\delta_s). \quad (3)$$

2.3. Solar radiation calculation

Estimation of monthly mean hourly GSR on a horizontal surface from daily solar radiation was found by Collares-Pereira and Rabl (1979).

$$I_h = r_t \cdot H_h \quad (4)$$

$$r_t = \pi/24 \cdot (a + b \cdot \cos\omega)\left(\frac{\cos\omega - \cos\omega_s}{\sin\omega_s - (\pi\omega_s/180)\cdot\cos\omega_s}\right) \quad (5)$$

where

$$a = 0.409 - 0.5016 \cdot \sin(\omega_s - 60) \quad (6)$$

$$b = 0.6609 - 0.4767 \cdot \sin(\omega_s - 60). \quad (7)$$

By taken account the formula of Liu and Jordan (1960), the hourly diffuse solar radiation is:

$$I_{d,h} = r_d \cdot H_{d,h} \quad (8)$$

$$r_d = \pi/24\left(\frac{\cos\omega - \cos\omega_s}{\sin\omega_s - (\pi\omega_s/180)\cdot\cos\omega_s}\right). \quad (9)$$

The monthly mean hourly direct solar irradiation on a horizontal surface:

$$I_{b,h} = I_h - I_{d,h}. \quad (10)$$

The monthly mean hourly direct solar irradiation on a inclined and oriented surface, it can be calculated by the next formula (Maia et al., 2014):

$$I_i = I_{b,h} \cdot R_b. \quad (11)$$

With

$$R_b = \frac{\cos i}{\cos i_z} \quad (12)$$

$$\cos i_z = \cos\varphi \cdot \cos\delta_s \cdot \cos\omega + \sin\varphi \cdot \sin\delta_s. \quad (13)$$

The monthly mean daily direct normal irradiation at *j* hour, was developed according to Pérez-Higueras et al. (2012)

$$H_i = \sum_{j=1}^{24} I_i(j) \cdot \Delta t \quad (14)$$

where $\Delta t = 1$ h.

For all the year, the results in Fig. 3 shows that the energy gains by the collector with two axis tracking (case 7) is most than the other cases of the collectors tracking systems. As can be seen in summer, the direct solar irradiation provided by horizontal N–S axis, polar N–S tracking and tilted tracking axis aperture to the south per latitude local (cases 3, 5 and 6) are superior to the horizontal E–W axis tracking and a tilted surface at an angle of 45° (cases 2 and 4), and in winter, the horizontal E–W axis tracking has

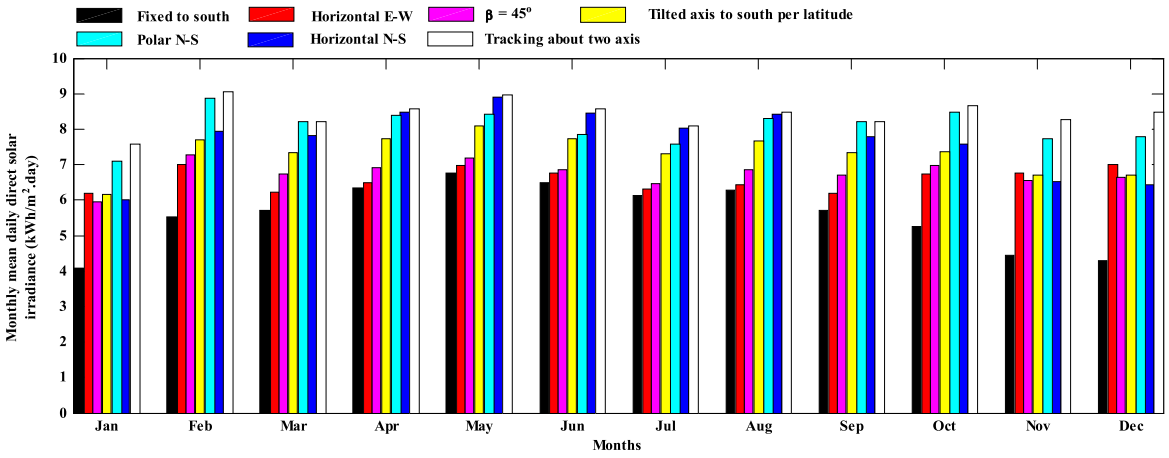

Fig. 3. Monthly mean daily direct solar radiation, in Tamanrasset city.

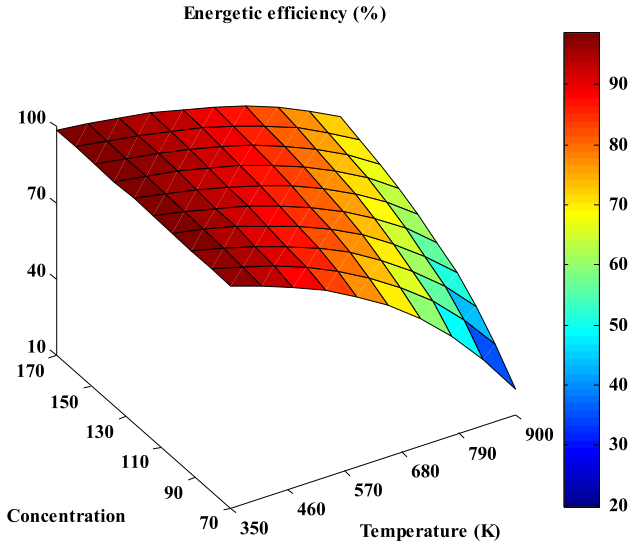

Fig. 4. Variation of the energetic efficiency according to the temperature of receiver for various values of the concentration.

the highest value than the horizontal N–S. While the fixed aperture to the south is the least efficient of all systems.

As shown in Fig. 3, we can see that the monthly mean direct solar irradiation for (case 7) it varies between 7 kWh/m^2·day and 9 kWh /m^2·day, however; from the cases (2, 3, 4, 5 and 6) the potential of direct solar irradiation is around 5 kWh /m^2·day and 8 kWh /m^2·day, and between 4 and 6 kWh/^{2}·day in the case (1).

The present study has shown that Tamanrasset is characterized by higher radiation over Algeria country and offers a promising opportunity to install solar thermal power projects that has been announced in the Algerian renewable energy program.

In the following sections, a detailed thermal performance of an ISCC under Tamanrasset climate is presented to highlight the advantages of implanting a solar thermal technology in such a region.

3. Description of the power plant components

Typical Integrated Solar Combined Cycle (ISCC) is consisted of a parabolic trough solar field and a fossil fuel combined cycle. The proposed ISCC in the present study is similar to the one that is in operation at Hassi R'mel. The combined cycle of the plant is made up of two gas turbines with an oversized steam turbine to provide large wide of operation. The solar field is made up of hundreds of parabolic trough collectors.

Table 2
Geometrical and optical parameters for the collector.

Parameters	Value
Characteristics of collector LS3:	
Aperture width (m)	7.76
Aperture area (m^2)	545
Collector length (m)	99
Optical Efficiency (%)	0.8
Concentration Ratio	82
Mirror reflectance	0.94
Receiver absorptivity	0.96
Receiver emittance	0.19
Characteristics of solar field:	
Alignment	North–South
Solar field area (m^2)	183,120
Number of collectors in each row	6
Number of lines	56
HTF inlet temperature (°C)	290
HTF outlet temperature (°C)	393

3.1. Parabolic trough collectors

The typical parabolic trough collector consists of reflector, receiver, tracking system and a metal structure. The reflector is made up of mirrors of high reflectivity. The receiver is a black metal tube, placed on the focal line of the concentrator, packed in a tube out of glass to limit the loss of heat by the convection. The axis of rotation of the parabolic trough collector in this study is directed north–south to maximize solar energy collection. The main technical characteristics of the selected collector are summarized in Table 2 (Derbal-Mokrane et al., 2012).

3.2. The solar field

The major performance parameter of the solar field is its efficiency (Gülen, 2015). The thermal efficiency of the collector depends on many parameters such as solar radiation intensity, optical performance of the collector and ambient conditions (Gülen, 2015). Fig. 4 shows the global thermal efficiency of the collector as function of receiver temperature and concentration ratio, where the values of concentration ratio here are between 70 and 170. From the simulation presented in Fig. 4, we can see that the higher the concentration ratio the higher the temperature and thus the higher is the thermal efficiency.

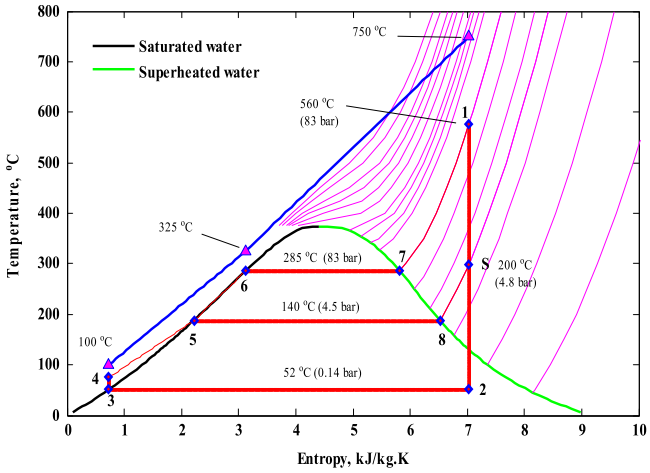

Fig. 5. Diagram of the Rankine water–steam cycle.

3.3. The power plant

As shown in Fig. 1, the proposed integrated solar combined cycle consists of the following components: solar field, two gas turbine units and a steam turbine. The main parameters of the power plant are illustrated in Tables 2 and 3 (Derbal-Mokrane et al., 2012; Khaldi, 2012). The solar field represents the key part of the plant. It consists of 56 loops and for each loop 6 collectors are arranged in parallel rows (type of LS-3). The collectors are single axis tracking aligned in north–south axis, thus tracking the sun from east to west. Therminol VP-1 heat transfer fluid is selected in the present analysis.

The power plant of the proposed scheme is a conventional combined cycle power plant with two gas turbine units (type SGT-800) with 40 MWe each, and a steam turbine (type SST-900) with a 80 MWe. Two identical single-pressure heat recovery steam generator (HRSG) are placed in parallel with a solar steam generator. During sunny periods, thermal energy from the solar field is added the heat of the gas turbines exhaust gases

The plant diagram illustrated in Fig. 5 shows Two Brayton cycles that are coupled to a one pressure level Rankine cycle via a heat recovery steam generator (HRSG). This latter is connected in parallel with a solar steam generator (Derbal-Mokrane et al., 2012).

4. Thermodynamic modeling of the ISCC

4.1. Modeling the solar field

A model has been developed to size the solar field. The selected location as it is highlighted above is "Tamanrasset" city. The geographical characteristics of this site are: 22.78° latitude, 2.52° longitude and 1385 Altitude.

The input data to the model are:

- Time: date (day of the year, hour).
- Location: latitude and longitude.
- Geometric: (Dimensions of the solar field).
- Optic: (coefficients of the absorption and the transmission of collector components).

The collected solar energy is depending on the collector optical performance and the angle of incidence between the beam solar and the surface of direct sun reflector (Badescu, 2002), on the other hand, the thermal power of a parabolic trough collector is affected by the heat losses of collector. Therefore, the useful energy gained by the collector $\dot{Q}_u$ can be expressed as:

Table 3
Technical data used in the ISCCs power plant calculation (Khaldi, 2012).

	Parameters inputs	Values
Gas Turbine	**Compressor:**	
	Inlet Ambient temperature (°C)	15
	Inlet pressure (bar)	1.013
	Compression ratio	20.2
	Isentropic Efficiency (%)	0.88
	Combustion chamber:	
	Inlet pressure (bar)	17.7
	Exhaust temperature (°C)	550
	Exhaust mass flow rate (kg/s)	120.20
	LHV of natural gas (kJ/kg)	45,778
	Turbine:	
	Isentropic Efficiency (%)	0.88
	Inlet temperature (°C)	1,200
	Outlet temperature (°C)	562
HRSG	Pinch temperature (°C)	25
	Approach temperature (°C)	25
	Fuel flow rate in DBs (kg/s)	0.66
	Inlet water temperature (°C)	60
HSSG	Inlet water temperature (°C)	195
	Inlet water pressure (bar)	93
	Exit steam temperature (°C)	372
	Steam mass flow rate (kg/s)	22.6
	HTF mass flow rate (kg/s)	205
Steam turbine	Inlet steam pressure (bar)	83
	Inlet steam temperature (°C)	560
	Outlet steam pressure (bar)	0.14

$$\dot{Q}_c = \dot{Q}_{abs} - \dot{Q}_{HeatLoss} \tag{15}$$

where

$$\dot{Q}_{abs} = A_c \cdot DNI \cdot \eta_o(i) \tag{16}$$

$\dot{Q}_{HeatLoss}$ is the sum of heat loss from the receivers $\dot{Q}_{HL,rec}$ and heat loss from piping to and from the solar field $\dot{Q}_{HL,pip}$:

$$\dot{Q}_{HeatLoss} = \dot{Q}_{HL,rec} + \dot{Q}_{HL,pip}. \tag{17}$$

According to Price et al. (2002), $\dot{Q}_{HL,pip}$ and $\dot{Q}_{HL,pip}$ are expressed by the following correlation equations:

$$\begin{aligned}\dot{Q}_{HL,rec} &= A + B \cdot \Delta T_f + C \cdot T_f^2 + D \cdot T_f^3 \\ &\quad + E \cdot DNI \cdot K(i) \cdot \cos i \cdot T_f^2 + \sqrt{V_w} \cdot (F + G \cdot \Delta T_f)\end{aligned} \tag{18}$$

$$\begin{aligned}\dot{Q}_{HL,pip} &= 1.693 \cdot 10^{-2} \cdot \Delta T - 1.683 \cdot 10^{-4} \cdot \Delta T^2 \\ &\quad + 6.78 \cdot 10^{-7} \cdot \Delta T^3\end{aligned} \tag{19}$$

A,B,C…F and G describe the heat losses of the heat collector element with ΔT_f as the temperature difference between the HTF and the ambient. The difference between the average field temperature and the ambient air temperature ΔT (°C) is given by Burkholder et al. (2009):

$$\Delta T = \frac{T_{f,out} + T_{f,in}}{2} - T_{amb}. \tag{20}$$

Table 4 presents the heat loss correlation coefficients for the 2008 PTR70 heat collection elements for LS-3 collector type.

Where the optical efficiency η_o is calculated by the following relation (Mokheimer et al., 2014):

$$\eta_o(i) = K(i) \cdot E_{Loss} \cdot R_{shad} \cdot \eta_{nom} \cdot f_{clean}. \tag{21}$$

The incidence angle modifier can be calculated by following equation (Mokheimer et al., 2014):

$$\begin{aligned}K(i) &= 1 - 2.2307 \cdot 10^{-4} \cdot i - 1.1 \cdot 10^{-4} \cdot i^2 \\ &\quad + 3.18596 \cdot 10^{-6} \cdot i^3 - 4.85509 \cdot 10^{-8} \cdot i^4.\end{aligned} \tag{22}$$

Table 4
2008 PTR70 heat loss coefficients.

Coefficients	Value
A	4.05
B	0.247
C	−0.00146
D	5.65E−06
E	7.62E−08
F	−1.70
G	0.0125

The total thermal energy $\dot{Q}_{sol,field}$ delivered by the solar field is:

$$\dot{Q}_{sol,field} = \dot{Q}_c \cdot N_c. \tag{23}$$

The performance of the solar field can be estimated using the thermal efficiency of the field (Derbal-Mokrane et al., 2012):

$$\eta_{sol,field} = \frac{\dot{Q}_c}{DNI \cdot A_{ap}}. \tag{24}$$

For the case of single-axis tracking (N–S), the angle of incidence is (Montes et al., 2011).

$$\cos i = \left[\cos i_z^2 + \cos\delta^2 \cdot \sin\omega^2\right]^{1/2}. \tag{25}$$

It should be noted that the heat losses proportional to the absorber surface, so depending on Burkholder et al. (2009), the measurements showed that the heat loss equal to 145 W/m^2 that is would lead to reduce in system efficiency and the size of the solar field power production. Nevertheless, the solar-to-electric efficiency of the ISCC plants is strongly affected by the cosine effect.

4.2. Modeling of the ISCC

Integrated solar combined cycle ISCC power plants generate electricity using the waste heat by gas turbine and solar steam generator to make steam to generate additional electricity via a steam turbine. ISCC power plants is well estimated using the Gas turbine cycle and Steam turbine cycle equations, which as found in Boyce (2002)

4.2.1. Gas turbine cycle model

The net work of the Gas turbine $W_{GT,net}$ is the difference between the actual compressor work W_C and the actual turbine work W_G. The work of the turbine and the compressor could be calculated respectively from Ibrahim et al. (2011):

$$W_G = \frac{C_{pg} \cdot T_{3'} \cdot \eta_T}{\eta_m}\left(1 - \frac{1}{\kappa_P^{\frac{\gamma_g - 1}{\gamma_g}}}\right) \tag{26}$$

$$W_C = \frac{C_{pa} \cdot T_{1'} \cdot \left(\kappa_P^{\frac{\gamma_a - 1}{\gamma_a}} - 1\right)}{\eta_T \cdot \eta_C} \tag{27}$$

where $\gamma_a = 1.4$ and $\gamma_g = 1.33$.

κ_P is the compressor pressure ratio; $\kappa_P = \frac{P_{2'}}{P_{1'}}$. Where C_{pa} and C_{pg} are the specific heats of air and flue gas, respectively, were calculated from the following equations:

$$C_{pa} = 1.0189 \times 10^3 - 0.13784T_a + 1.9843 \times 10^{-4}T_a^2 + 4.2399 \times 10^{-7}T_a^3 - 3.7632 \times 10^{-10}T_a^4 \tag{28}$$

$$C_{pg} = 1.8083 - 2.3127 \times 10^{-3}T + 4.045 \times 10^{-6}T^2 - 1.7363 \times 10^{-9}T^3 \tag{29}$$

where $T_a = \frac{T_{2'} + T_{1'}}{2}$ is the air temperature at the compressor entrance is assumed to be equal to the ambient air temperature $T_{1'} = T_{amb}$.

$T_{2'}$ is the outlet temperature of the compressor, it can be expressed as:

$$T_{2'} = T_{1'} \cdot \left(1 + \frac{\kappa_P^{\frac{\gamma_a - 1}{\gamma_a}} - 1}{\eta_C}\right). \tag{30}$$

As defined in, the mass flow rate of exhaust gases from the gas turbine and the ratio of mass flow in a combustion chamber are as follows:

$$\dot{m}_g = \dot{m}_a + \dot{m}_f \tag{31}$$

$$f = \frac{\dot{m}_f}{\dot{m}_a} = \frac{C_{pg} \cdot T_{3'} - C_{pa} \cdot T_{2'}}{LHV - C_{pg} \cdot T_{3'}}. \tag{32}$$

By combining Eqs. (31) and (32), we can write:

$$\dot{m}_a = \frac{\dot{m}_g}{(1+f)} = \frac{\dot{m}_g \cdot \left(LHV - C_{pg} \cdot T_{3'}\right)}{LHV - C_{pa} \cdot T_{2'}}. \tag{33}$$

The net work of the Gas turbine $W_{GT,net}$ can be calculated by the following equation:

$$W_{GT,net} = W_G - W_C. \tag{34}$$

The net power output and the thermal efficiency of the gas turbine $N_{GT,net}$:

$$N_{GT,net} = \dot{m}_a \cdot W_{GT,net} \tag{35}$$

$$\eta_{GT,net} = \frac{N_{GT,net}}{Q_{add}} \tag{36}$$

where Q_{add} is total heat supplied in the combustion, it can be given by:

$$Q_{add} = C_{pg} \cdot (T_{3'} - T_{2'}). \tag{37}$$

4.2.2. Steam turbine cycle model

The performance of the steam Rankine cycle based on mass and energy conservation equations has been performed according to the mathematical model mentioned down (Safarian and Aramoun, 2015).

Firstly, we use heat balance around the Deaerator (Fig. 1) to find Y:

$$Y = \frac{h_5 - h_4}{h_S - h_4}. \tag{38}$$

Secondly, the air to steam ratio is found from heat balance around the heat exchanger:

$$\frac{\dot{m}_a}{\dot{m}_{steam}} = \frac{h_5 - h_1}{C_{pa}(T_{4'} - T_{1'})} \tag{39}$$

where the net work of steam turbine is:

$$W_{ST} = \dot{m}_{steam} \cdot [Y \cdot (h_1 - h_S) + (1 - Y)(h_1 - h_2)]. \tag{40}$$

The heat required from the condenser is calculated as:

$$Q_C = \dot{m}_{steam} \cdot (1 - Y)(h_3 - h_2). \tag{41}$$

The feed water pump work is:

$$W_{FP} = \dot{m}_{steam} \cdot (h_4 - h_3). \tag{42}$$

The net power of steam cycle output ($N_{net,ST}$) and the efficiency of the steam cycle (η_{ST}) are expressed in the following equations (Bartlett, 1958):

$$N_{net,ST} = W_{ST} \cdot \eta_m - \frac{W_{FP}}{\eta_p} \tag{43}$$

$$\eta_{net,ST} = \frac{N_{net,ST}}{\dot{Q}_{solar,field} + \dot{Q}_{ex}} \tag{44}$$

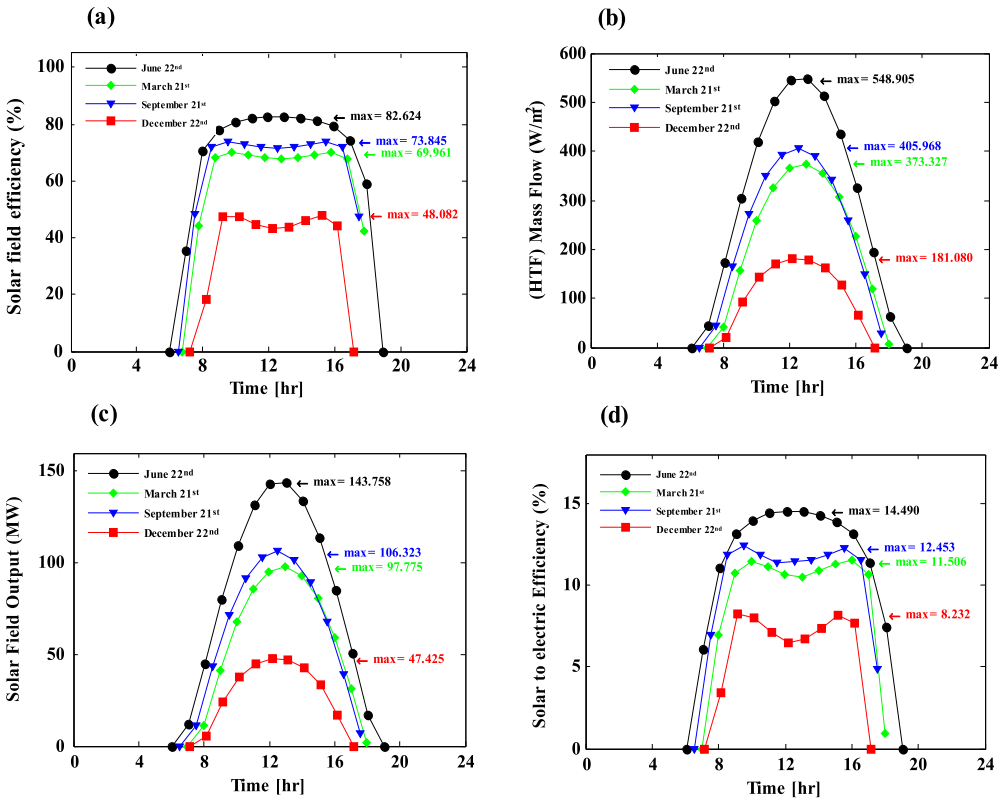

Fig. 6. Variation of: (a) solar field efficiency, (b) HTF mass flow, (c) solar field output and (d) solar to electric efficiency on four typical days of a year.

where the isentropic efficiencies of the steam turbine (η_m) and the pump (η_p) are 80% and 85%, respectively.

In order to calculate inlet/outlet the enthalpy and the pressure of steam in the most important points of the Rankine water–steam cycle, as shown in Fig. 2, we used the international tables of water properties (saturated region and superheated steam region) from the reference (Çengel et al., 2015).

Point (1): Inlet enthalpy and entropy at the steam turbine are determined by the inlet pressure and inlet temperature of the steam:

$$\begin{cases} h_1 = h(P_1 = 83\ \text{bar}, T_1 = 560\ ^\circ\text{C}) \\ h_1 = 3661\ \text{kJ/kg} \\ S_1 = 7.027\ \text{kJ/kg} \cdot \text{K}. \end{cases}$$

Point (2) and (S): The exit enthalpy and pressure may be determined from the outlet temperature of the steam at the steam turbine:

$$\begin{cases} h_s = h(P_s = 4.8\ \text{bar}, T_s = 200\ ^\circ\text{C}) \rightarrow h_s = 2862\ \text{kJ/kg} \\ h_2 = h(T_2 = 52\ ^\circ\text{C}) \rightarrow h_2 = 2397.59\ \text{kJ/kg} \\ P_2 = P(T_2 = 52\ ^\circ\text{C}) \rightarrow P_2 = 0.14\ \text{bar}. \end{cases}$$

Point (3): It is assumed that there is no pressure drop in the steam side of the condenser (turbine exhaust pressure equal to the condensing pressure):

$$\begin{cases} h_3 = h_2(T_3 = 52\ ^\circ\text{C}) \\ h_3 = 217.6\ \text{kJ/kg} \\ P_3 = 0.14\ \text{bar} \\ \nu_3 = 0.001013\ \text{m}^3/\text{kg}. \end{cases}$$

Point (4): The enthalpy at the pump is evaluated using the outlet pressure and outlet enthalpy of the condenser:

$$\begin{cases} h_4 = \nu 3 \cdot (P_4 - P_3) + h_3 \\ h_4 = 224.55\ \text{kJ/kg} \\ P_4 = 7\ \text{bar}. \end{cases}$$

Point (5): The enthalpy of the outlet deaerator is defined from the outlet temperature and outlet pressure of the steam:

$$\begin{cases} h_5 = h(P_5 = 4.5\ \text{bar}, \text{T}_5 = 140\ ^\circ\text{C}) \\ h_5 = 619.83\ \text{kJ/kg}. \end{cases}$$

4.3. Modeling of the ISCC

The thermal efficiency of the ISCCs is calculated taking into account solar energy contribution (Vasquez Padilla, 2011).

$$\eta_{ISCC} = \frac{N_{ISCC}}{\dot{m}_f \cdot LHV + \dot{Q}_{sol,field}} \tag{45}$$

where N_{ISCC} is the power production by the ISCC power plant, it is given by Derbal-Mokrane et al. (2012).

$$N_{ISCC} = 2 \cdot N_{GT} + N_{ST} \tag{46}$$

where the solar power production ($N_{sol,el}$) and the solar-to-electric efficiency ($\eta_{sol,el}$) are defined as: (Franchini et al., 2013)

$$N_{sol,el} = N_{ISCC} - \eta_{CC} \cdot Q_{fuel} \tag{47}$$

$$\eta_{sol,el} = \frac{N_{sol,el}}{DNI \cdot A_{ap}}. \tag{48}$$

4.4. Modeling of the IGCC

In this paper, the performance of ISCC has been validated by comparing the IGCC simulation results. Therefore, the IGCC performance can be calculated by deleting all others auxiliaries which, are the sum of all of the power consumptions of the additional components, including the auxiliary air compressor and various compressors and pumps as shown in Eqs. (39) and (40). The net

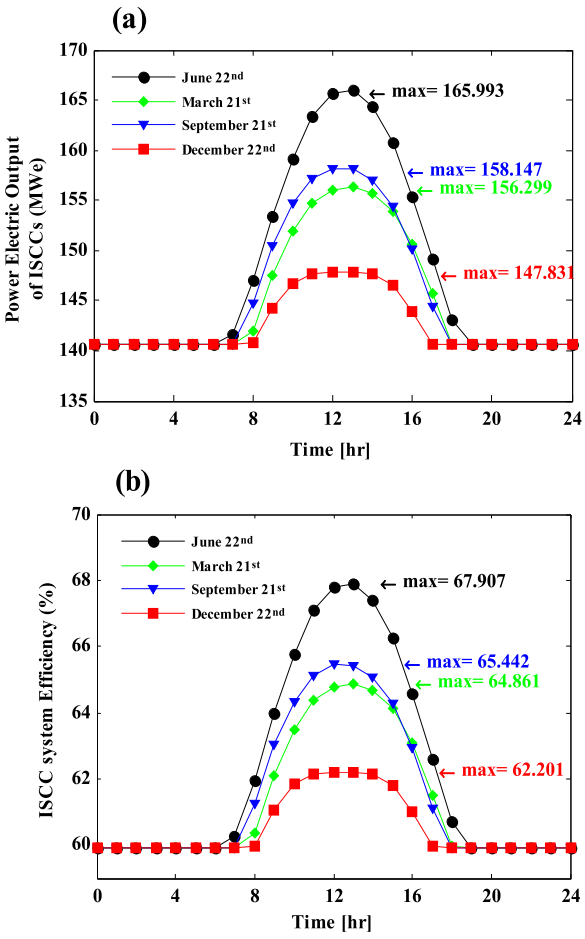

Fig. 7. Hourly power electric output and efficiency of ISCC on four typical days of a year.

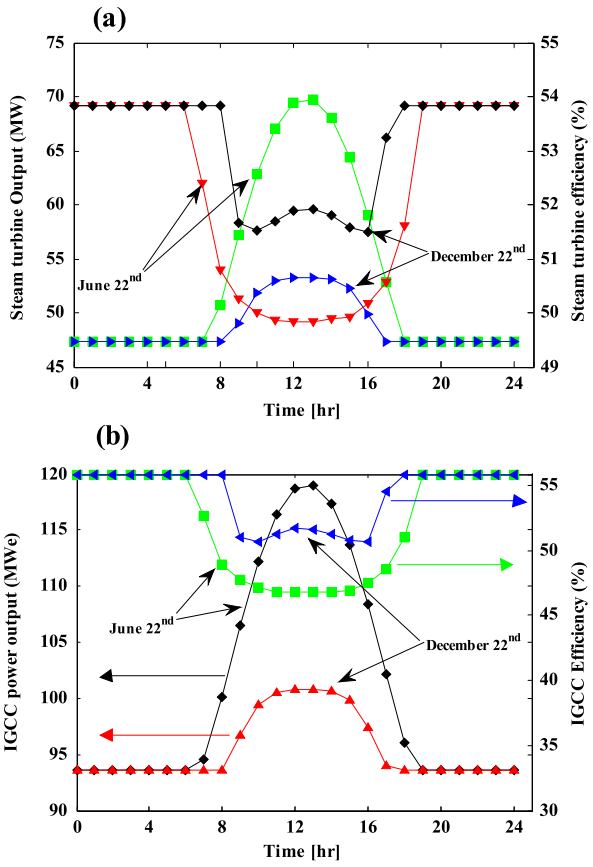

Fig. 8. Hourly of: (a) ST power output and efficiency, (b) IGCC output and efficiency on four typical days of a year.

IGCC power output and efficiency were defined as follows: (Emun et al., 2010)

$$N_{IGCC} = 2 \cdot N_{GT} + N_{ST} - N_{AUX} \tag{49}$$

$$\eta_{IGCC} = \frac{N_{IGCC}}{\dot{m}_f \cdot LHV}. \tag{50}$$

5. Simulation and discussion of the results

A thermodynamic model has been developed based on the modeling described above. This includes the modeling of solar radiation, the solar field and the power conversion cycles.

As the performance of the solar field has strong effect on the ISCC performance, it is important to analysis its efficiency. Form Fig. 6(a) we can conclude that the efficiency of the solar field might reach up to 82.62% in summer. However, it can be lower than 48.08% in winter. In spring and autumn the solar field efficiency can reach 73.84% and 69.96% respectively.

Indeed the solar field works in variable flow strategy, and thus the inlet and outlet temperatures of the HTF are set constant. In this study, the inlet and outlet HTF temperatures in the field are 290 °C and 393 °C respectively. The variation of the HTF mass flow is shown in Fig. 6(b). It is obvious that the higher the solar radiation the higher is the mass flow rate of the HTF. The increase in solar radiation results in an increase in absorbed solar energy and thus the solar field thermal energy gain is increase (see Fig. 6(b)).

We have analyzed with awareness the performance of the ISCC during a year. Concerning the overall performance of the power plant, the total energy production, as shown in Fig. 7(a), could reach to the peak value of 165 MW in the first period, and a minimum value of 140 MW is observed during the low radiation periods.

The ISCC is working in boosting mode and thus the higher the solar radiation the higher the electricity production by the power plant. This is due to the increase of steam mass flow in the heat recovery steam generator (HRSG). The overall efficiency of the ISCC is an important factor. From Fig. 7(b), it can be seen that the overall efficiency is very interesting since it can reach the limit of 68%.

To highlight the efficiency of converting solar energy, solar to electricity efficiency in the four seasons is simulated. During winter, the solar to electricity efficiency decreases at noon even the DNI reaches its maximum. This is due to solar angle of incidence. This is not the case during summer, solar to electricity efficiency can reach 14.490% (Fig. 6(d)). As shown in Fig. 8(a), the total steam turbine output is equal to 69 MW at the design point which means an increase in electricity generation by about 23 MW compared to 47 MW at night, while the steam turbine efficiency is 53% in summer and 51% in winter at the design point, and 50% at night. which means that the increase of thermal energy by solar field leads to a decrease in the efficiency of steam turbine and vice versa.

Separating the auxiliaries effects in IGCC is useful for analyzing ISCC system performance. Obviously, there are a great variations in the IGCC performance compared to the ISCC power plant. In Fig. 8(b), the power produced by the IGCC reach to the peak value of 119 MW in the summer with efficiency of up to 46% and 100 MW in winter with efficiency about 51%.

We have also observed that the day of the year may be divided into three main periods. The peak-radiation period from 11 am to 1 pm. The moderate radiation period that includes 9:00–11:00 am

Table 5
A comparison study showing good agreement with experimental data.

Hours	Experimental data (for 21 June) Net production from ISCC (MWh)	Present model (for 21 June) Net production from ISCC (MWh)	Experimental data (for 21 December) Net production from ISCC (MWh)	Present model (for 21 December) Net production from ISCC (MWh)
1	151.361	140.6347	128.577	140.6347
2	151.711	140.6347	129.869	140.6347
3	152.033	140.6347	131.100	140.6347
4	152.354	140.6347	132.336	140.6347
5	152.500	140.6347	133.578	140.6347
6	152.500	140.6347	131.141	140.6347
7	152.500	141.5955	137.230	140.6347
8	152.500	147.0784	135.619	140.6347
9	152.500	153.4448	134.615	143.6684
10	152.500	159.1656	133.489	146.4125
11	152.431	163.3818	131.540	147.5648
12	151.932	165.6842	130.834	147.8233
13	151.691	165.9927	130.185	147.8342
14	151.462	164.3344	129.338	147.6749
15	151.612	160.7026	129.367	146.8058
16	152.027	155.3924	130.392	144.4603
17	151.102	149.1075	130.908	140.9447
18	151.195	143.0955	126.250	140.6347
19	151.317	140.6347	122.395	140.6347
20	151.409	140.6347	123.928	140.6347
21	151.500	140.6347	125.103	140.6347
22	151.619	140.634	126.287	140.6347
23	151.707	140.6347	127.593	140.6347
24	151.797	140.6347	128.776	140.6347

and 1–3 pm. The low radiation period that comprises 7–9 am and 3–5 pm.

In order to validate the developed model, the results of the current model are compared against measured data of Hassi R'mel power plant, as shown in Table 5. The comparison study shows good agreement with measured data.

6. Conclusion

The present study is aimed at a detailed assessment of the Integrated Solar Combined Cycle (ISCC) technology under tropical climate. Thus, a thermodynamic model has been developed to predict their thermal performance in Tamanrasset (southern of Algeria). Since solar radiation data are not available in most Algerian regions, we have first developed a linear regression model based on sunshine duration to assess the direct solar radiation intensity at the selected site. After that, the solar field is modeled taking into consideration the optical and thermal proprieties of the collector. The thermodynamic model of the ISCC is then developed based on mass and energy balance of each component of the power plant.

This model is used to simulate the thermal performance of the power plant. The solar field performances at different seasons of the year are analyzed. The variation of various operation parameters including heat transfer fluid flow rate and the solar incident angle were examined. The overall performances of the ISCC are also investigated. The solar to electricity efficiency on four typical days has been discussed. It has been found that the peak solar to electricity efficiency in summer can reach up to 14.4% while it is around 8% in winter due to the lower solar radiation intensity that is also affected by the solar incident angle. The simulation has shown that the overall thermal efficiency of the ISCC could reach more than 60%. In other word, the higher the solar radiation the higher is the electricity production and the higher is the overall thermal efficiency.

Therefore, the results obtained in the present study provide some guidelines and suggestions for the development of integrated solar combined cycle technology that might help meeting the focus on Algerian renewable energy program that is announced in 2011.

References

Allani, Y., Favrat, D., Von Spakovsky, M.R., 1997. CO2 mitigation through the use of hybrid solar-combined cycles. Energy Convers. Manage. 38 (Supplement), S661–S667.

Badescu, V., 2002. 3D isotropic approximation for solar diffuse irradiance on tilted surfaces. Renew. Energy 26, 221–233.

Baghernejad, A., Yaghoubi, M., 2011. Exergoeconomic analysis and optimization of an Integrated Solar Combined Cycle System (ISCCS) using genetic algorithm. Energy Convers. Manage. 52, 2193–2203.

Bakos, G.C., Parsa, D., 2013. Technoeconomic assessment of an integrated solar combined cycle power plant in Greece using line-focus parabolic trough collectors. Renew. Energy 60, 598–603.

Bartlett, R.L., 1958. Steam Turbine Performance and Economics. McGraw-Hill, New York.

Behar, O., Kellaf, A., Mohamedi, K., Belhamel, M., 2011. Instantaneous performance of the first Integrated Solar Combined Cycle System in Algeria. Energy Procedia 6, 185–193.

Besarati, S.M., Padilla, R.V., Goswami, D.Y., Stefanakos, E., 2013. The potential of harnessing solar radiation in Iran: Generating solar maps and viability study of PV power plants. Renew. Energy 53, 193–199.

Boyce, M.P., 2002. Handbook for Cogeneration and Combined Cycle Power Plants. ASME Press, New York.

Burkholder, F., Kutscher, C.F., National Renewable Energy, L., 2009. Heat Loss Testing of Schott's 2008 PTR70 Parabolic Trough Receiver. National Renewable Energy Laboratory, Golden, CO.

Cau, G., Cocco, D., Tola, V., 2012. Performance and cost assessment of Integrated Solar Combined Cycle Systems (ISCCSs) using CO2 as heat transfer fluid. Sol. Energy 86, 2975–2985.

Çengel, Y.A., Boles, M.A., Kanoglu, M., 2015. Thermodynamics: an engineering approach.

Collares-Pereira, M., Rabl, A., 1979. The average distribution of solar radiation-correlations between diffuse and hemispherical and between daily and hourly insolation values. Sol. Energy 22, 155–164.

Derbal-Mokrane, H., Bouaichaoui, S., Gharbi, N.E., Belhamel, M., Benzaoui, A., 2012. Modeling and numerical simulation of an Integrated Solar Combined Cycle System in Algeria. Procedia Eng. 33, 199–208.

Dersch, J., Geyer, M., Herrmann, U., Jones, S.A., Kelly, B., Kistner, R., Ortmanns, W., Pitz-Paal, R., Price, H., 2004. Trough integration into power plants — a study on the performance and economy of integrated solar combined cycle systems. Energy 29, 947–959.

Duffie, J.A., Beckman, W.A., 1991. Solar Engineering of Thermal Processes. J. Wiley.

El Mghouchi, Y., El Bouardi, A., Choulli, Z., Ajzoul, T., 2014. New model to estimate and evaluate the solar radiation. Int. J. Sustain. Built Environ. 3, 225–234.

Emun, F., Gadalla, M., Majozi, T., Boer, D., 2010. Integrated gasification combined cycle (IGCC) process simulation and optimization. Comput. Chem. Eng. 34, 331–338.

Franchini, G., Perdichizzi, A., Ravelli, S., Barigozzi, G., 2013. A comparative study between parabolic trough and solar tower technologies in Solar Rankine Cycle and Integrated Solar Combined Cycle plants. Sol. Energy Part C 98, 302–314.

Goswami, D.Y., Kreith, F., Kreider, J.F., Kreith, F., 2000. Principles of Solar Engineering. Taylor & Francis, Philadelphia, PA.

Gülen, S.C., 2015. Second law analysis of integrated solar combined cycle power plants. J. Eng. Gas Turbines Power 137, 051701.
Ibrahim, T.K., Rahman, M.M., Abdalla, A.N., 2011. Gas turbine configuration for improving the performance of combined cycle power plant. Procedia Eng. 15, 4216–4223.
Kane, M., Favrat, D., 1999. Approche de conception et d'optimisation de centrale solaire intégrée à cycle combiné inspirée de la méthode du pincement (partie II: réseau d'échangeurs de chaleur). Int. J. Therm. Sci. 38, 512–524.
Khaldi, F., 2012. Energy and exergy analysis of the first hybrid solar-gas power plant in Algeria. In: ECOS. pp. 26–29.
Li, Y., Yang, Y., 2014. Thermodynamic analysis of a novel integrated solar combined cycle. Appl. Energy 122, 133–142.
Li, Y., Yang, Y., 2015. Impacts of solar multiples on the performance of integrated solar combined cycle systems with two direct steam generation fields. Appl. Energy 160, 673–680.
Liu, B.Y.H., Jordan, R.C., 1960. The interrelationship and characteristic distribution of direct, diffuse and total solar radiation, U.S.
Maia, C.B., Ferreira, A.G., Hanriot, S.M., 2014. Evaluation of a tracking flat-plate solar collector in Brazil. Appl. Therm. Eng. 73, 953–962.
Manente, G., 2016. High performance integrated solar combined cycles with minimum modifications to the combined cycle power plant design. Energy Convers. Manage. 111, 186–197.
Mokheimer, E.M.A., Dabwan, Y.N., Habib, M.A., Said, S.A.M., Al-Sulaiman, F.A., 2014. Techno-economic performance analysis of parabolic trough collector in Dhahran, Saudi Arabia. Energy Convers. Manage. 86, 622–633.
Montes, M.J., Rovira, A., Muñoz, M., Martínez-Val, J.M., 2011. Performance analysis of an integrated solar combined cycle using direct steam generation in parabolic trough collectors. Appl. Energy 88, 3228–3238.
Pérez-Higueras, P.J., Rodrigo, P., Fernández, E.F., Almonacid, F., Hontoria, L., 2012. A simplified method for estimating direct normal solar irradiation from global horizontal irradiation useful for CPV applications. Renew. Sustain. Energy Rev. 16, 5529–5534.
Popov, D., 2014. Innovative solar augmentation of gas turbine combined cycle plants. Appl. Therm. Eng. 64, 40–50.
Price, H., Lüpfert, E., Kearney, D., Zarza, E., Cohen, G., Gee, R., Mahoney, R., 2002. Advances in parabolic trough solar power technology. J. Sol. Energy Eng. 124, 109.
Raafat, S.W., 1994. Maadi: Society and History in a Cairo Suburb. Palm Press, Zamalek, Cairo, Egypt, pp. 1904–1962.
Rovira, A., Barbero, R., Montes, M.J., Abbas, R., Varela, F., 2016. Analysis and comparison of Integrated Solar Combined Cycles using parabolic troughs and linear Fresnel reflectors as concentrating systems. Appl. Energy 162, 990–1000.
Safarian, S., Aramoun, F., 2015. Energy and exergy assessments of modified Organic Rankine Cycles (ORCs). Energy Rep. 1, 1–7.
Vasquez Padilla, R., (2011) Simplified methodology for designing parabolic trough solar power plants [Online]. Available: http://scholarcommons.usf.edu/etd/3390.
Zhu, G., Neises, T., Turchi, C., Bedilion, R., 2015. Thermodynamic evaluation of solar integration into a natural gas combined cycle power plant. Renew. Energy 74, 815–824.